**Article ID:** 1671-3664(2005)02-0213-16

# Neural network analysis of overturning response under near-fault type excitation

Nikos Gerolymos†, Marios Apostolou‡ and George Gazetas§

*School of Civil Engineering, National Technical University, Athens, Greece*

**Abstract:** Under strong seismic excitation, a rigid block will uplift from its support and undergo rocking oscillations which may lead to (complete) overturning. Numerical and analytical solutions to this highly nonlinear vibration problem are first highlighted in the paper and then utilized to demonstrate how sensitive the overturning behavior is not only to the intensity and frequency content of the base motion, but also to the presence of strong pulses, to their detailed sequence, and even to their asymmetry. Five idealised pulses capable of representing "rupture–directivity" and "fling" affected ground motions near the fault, are utilized to this end : the one–cycle sinus, the one–cycle cosinus, the Ricker wavelet, the truncated (T)–Ricker wavelet, and the rectangular pulse "Overturning–Acceleration Amplification" and "Rotation" spectra are introduced and presented. Artificial neural network modeling is then developed as an alternative numerical solution. The neural network analysis leads to closed–form expressions for predicting the overturning failure or survival of a rigid block, as a function of its geometric properties and the characteristics of the excitation time history. The capability of the developed neural network modeling is validated through comparisons with the numerical solution. The derived analytical expressions could also serve as a tool for assessing the destructiveness of near–fault ground motions, for structures sensitive to rocking with foundation uplift.

**Keywords:** overturning; uplifting; pulse; near–fault motion; neural network; rocking spectrum; Kocaeli records

## 1 Introduction

The discovery on the ground surface after an earthquake of slender blocks standing vertically or lying on their side (overturned), has for many years provided upper–bound and lower–bound estimates of the peak ground acceleration. The fallacy that the acceleration needed to just overturn a block is the one obtained from moment equilibrium between the statically–applied inertia force and the weight of the block, prevailed for nearly a century and has led to the universal establishment of unrealistically low levels of ground acceleration (of the order of 0.05g to 0.10g, even in areas of high seismicity). Unfortunately, much greater acceleration levels are needed for overturning under *seismic* shaking, especially for large blocks and at high frequencies. Ironically, this was already known (even if incompletely) as early as 1893 (Milne and Omori), while by 1927 Kirkpatrick had published a simple formula for estimating the "dynamic" overturning acceleration, which captured the role of the basic problem parameters with sufficient degree of realism (Eq. (7) herein).

**Correspondence to**: Nikos Gerolymos, School of Civil Engineering, National Technical University, Athens, Greece
Fax: 30-210-6007699
E-mail: gerolymos@mycosmos.gr
†Post-doctoral Research Engineer; ‡Ph.D. Student; §Professor
**Received** 2005-05-02; **Accepted** 2005-07-14

In the subsequent 40 years the lack, or scarcity, of accelerographs prompted many researchers and earthquake engineers to study the overturning behavior of slender bodies. However, the dynamic character of the overturning behavior was not widely understood by the engineering community until Housner's (1963) publication, in which he derived overturning criteria and showed the importance of both frequency of excitation and size of structure.

The subject of overturning of blocks and structures under seismic excitation has in recent years received renewed attention, fueled by a variety of structural and non-structural elements (ranging from ancient columns, to electrical transformers, to trains, to buildings) toppled in numerous recent earthquakes, including those of Kocaeli 1999, Athens 1999, and Düzce 1999 (Apostolou and Gazetas, 2005). Makris and Roussos (1998) and Anooshehpoor *et al.* (1999), in particular, focused on the transient response of rigid blocks under near–fault ground shaking. They found that distinguishable long–duration pulses inherent to such shaking may be particularly detrimental to the rocking response of slender structures. Many examples of such pulses have been uncovered in near–fault records of recent $M_s \geq 6.5$ earthquakes, such as the Imperial Valley 1979, Erzincan 1992, Northridge 1994, Kobe 1995, Kocaeli 1999, and Chi–Chi 1999. These pulses are the result of two effects: the "forward rupture directivity" effect and "permanent

offset" (or "fling") effect (Somerville, 2003; Hisada and Bielak, 2003; Abrahamson, 2001).

In light of the above, the present study investigates the overturning potential of near-fault ground motion, represented for simplicity and clarity with the following idealized pulses : the Ricker-wavelet, the (truncated) T-Ricker wavelet, the one-cycle sinus, the one-cycle cosinus, and the rectangular half-cycle pulse. Their time histories are plotted in Fig. 1. The capability of these idealised pulses to represent actual near–fault records has been shown by Makris and Roussos (2000) and it is further demonstrated in this paper.

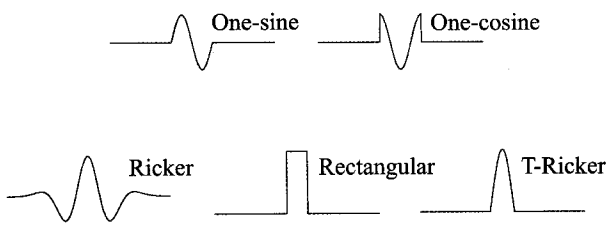


**Fig. 1 Idealized pulses utilized in this study to represent near-fault ground motion**

## 2 Overturning response of rigid blocks

Consider a rigid rectangular block with aspect ratio $b/h$ (half width / half height ratio) simply supported on a rigid base, which is oscillating horizontally. The coefficient of friction is adequately large so that sliding is prevented. As long as the overturning moment of the inertia force ($ma_g h$), where $a_g = \alpha_g(t)$ = the base acceleration, does not exceed the restoring moment ($mgb$) about the base edge, the block remains attached to, and follows the oscillation of, the base. As soon as the restoring moment $mgb$ is exceeded, uplifting occurs setting the block on rocking motion. The system configuration is illustrated in Fig 2.

Under pseudo-static conditions, once uplifting is initiated about the corner point, the body will unavoidably overturn. In other words, the critical acceleration for uplifting is identical with the minimum required to *statically* overturn the block. It is given by the so called "West formula" (Milne and Omori, 1893); in units of g:

$$\alpha_{\text{over,stat}} \equiv \alpha_c = \frac{b}{h} \tag{1}$$

On the other hand under dynamic base excitation, exceeding $\alpha_c$ simply initiates rocking. Whether the block will eventually overturn or not depends on its size and slenderness, as well as on the nature and intensity of ground shaking. The response is determined by the governing equation of motion :

$$\ddot{\theta}(t) = -p^2\left\{\sin\left[\theta_c \operatorname{sgn}\theta(t) - \theta(t)\right] + \alpha_g \cos\left[\theta_c \operatorname{sgn}\theta(t) - \theta(t)\right]\right\} \tag{2}$$

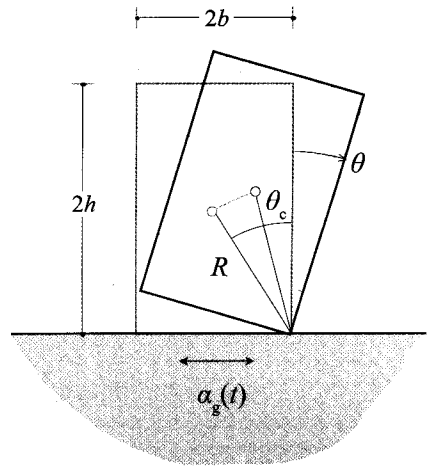


**Fig. 2 Rocking on a rigid base due to earthquake shaking: system configuration.**

where: $\theta(t) < 0$ $(or > 0)$ denotes the angle of rotation about $O$ (or, respectively, about $O'$); $\theta_c = \arctan(b/h)$ is the angle shown in Fig. 2; and $p = \sqrt{mgR/I_o}$ is a characteristic frequency parameter of the block; $R$ is half the diagonal of the block. For a solid rectangular block the moment of inertia about its pivot point is $I_o = (4/3)\,mR^2$, and therefore $p = \sqrt{3g/4R}$.

When a rigid body is rocking back and forth about its pivot points, it impacts the ground and loses a part of its kinetic energy, even in a purely elastic impact. Its angular velocity right after the impact (at time $t_o^+$) is a fraction of that just prior to impact (at time $t_o^-$):

$$\dot{\theta}^2(t_o^+) = r\ \dot{\theta}^2(t_o^-) \tag{3}$$

where $r$ is known in the literature as the coefficient of *restitution*. An upper bound of $r$ can be obtained by applying the momentum preservation and neglecting energy loss during impact :

$$r = \left(1 - \frac{3}{2}\sin^2\theta_c\right)^2 \tag{4}$$

In reality, some additional energy is lost, depending on the nature of the materials at the impact surface.

The rocking response of a rigid block can be obtained at any time increment through numerical integration of Eqs. (2) and (3). For slender blocks however, Eq. (2) can be reduced to the following piecewise linearized and dimensionless form:

$$\ddot{\Theta} - \Theta = -A\cos(\Omega_0\tau + \Psi) - \operatorname{sgn}\Theta \tag{5}$$

in which $\Theta = \theta/\theta_c$, $A = \alpha_g/\alpha_c$, $\Omega_0 = \omega_E/p$ , $\tau = pt$ and $\Psi$ are respectively the dimensionless rotational angle, the "dynamic" amplification of the overturning acceleration, the frequency ratio, time and phase shift. For harmonic excitation the analytical solution of Eq. (5) is (Spanos and Koh, 1984):

$$\Theta^{+}(\tau)=\alpha^{+}\sinh\tau+\beta^{+}\cosh\tau+1+\gamma\cos(\Omega\tau+\Psi),\quad \theta>0 \tag{6a}$$

$$\Theta^{-}(\tau)=\alpha^{-}\sinh\tau+\beta^{-}\cosh\tau-1+\gamma\cos(\Omega\tau+\Psi),\quad \theta<0 \tag{6b}$$

where $\alpha^{+}$, $\alpha^{-}$, $\beta^{+}$, $\beta^{-}$ are integration constants and $\gamma=-A/\left(1+\Omega^{2}\right)$.

The computed time-history of the rocking response with one of the above-discussed procedures can be used to derive minimum acceleration levels for overturning. To this end it should be postulated that the required time for marginal overturning to occur is infinitely large.

## 3 Sensitivity to problem parameters

### 3.1 Block size and excitation frequency

The major outcome of the nonlinear nature of rocking motion is that for a specific type of ground motion, the required acceleration for overturning is a sensitive function of both the block size and the excitation frequency. This has been recognized by many researchers since more than a century (Milne and Omori, 1893). Eighty years ago, Kirkpatrick (1927), assuming small rotations and slender structures, was the first to quantify the effects of the two afore mentioned parameters on the overturning response. For a sinusoidal excitation he derived analytically the necessary acceleration for overturning :

$$a_{\text{over}}=\frac{b}{h}g\sqrt{1+\left(\frac{\omega_{\text{E}}}{p}\right)^{2}} \tag{7}$$

Housner (1963) studied thoroughly the overturning response under pulse-type and white-noise excitation and re-derived Eq. (7) for the case of a half-sine pulse. This simplified formula is a good approximation of the exact solution for steady-state harmonic excitation. However, for the case of a half-sine pulse, it was based on a conceptually incorrect overturning criterion ($\theta(t)=\theta_c$ when the pulse expires) and it turns out to be unconservative (Makris and Roussos, 1998). It will be seen in the sequel, that a rocking block may temporarily experience $\theta(t)>\theta_c$ by an ample margin, without failure.

Using cycloidal pulses Makris and Roussos (1998, 2000) unveiled the detrimental role of long-period pulses inherent in near-fault ground shaking. Using the simplified solution (Eq. (6)) they derived a closed-form expression for the minimum acceleration amplitude of a one-sine pulse for overturning to occur. Their analytical and our numerical solution are compared in Fig. 3(a) for $r$=0.8.

Evidently, increasing the frequency $\Omega=\omega_{\text{E}}/p\cong 5.45$ of the pulse and the size of the block (i.e. decreasing the parameter $p$) affects favourably the overturning response. Note that for sufficiently high frequency pulses the required acceleration for overturning can be substantially larger than the critical static value $\alpha_c=b/h$. As an example, for excitation period of 0.3 sec and block diameter of 0.5 m the frequency ratio is $\Omega=\omega_{\text{E}}/p\cong 5.45$ which leads to a minimum acceleration about 4 times the static acceleration $(A\cong 4)$. On the other hand, an excitation period of 1 sec could be regarded as a static loading as for the same block diameter it results to a minimum acceleration that tends to the static value ($A\cong 1.2$).

The profoundly nonlinear-dynamic nature even of the piecewise linear system is not reflected only on the minimum acceleration amplitudes. In Fig. 3 notice that a one-cycle pulse may overturn a block either after one impact (mode 1) or without impact at all (mode 2). A "safe region" is revealed between the two modes, meaning that while the block overturns for a certain level of shaking, it surprisingly remains standing when the amplitude increases.

### 3.2 Asymmetry and detailed sequence of pulses

In the foregoing, the sensitivity of the overturning response to the size of the block and the frequency of excitation was discussed under a one-cycle sinus pulse. In Fig. 3(b) the overturning spectrum for the case of a one-cycle cosinus pulse is presented for the analytical solution of Makris and Zhang and our numerical solution of Eq. (5). The difference in the block behavior in response to the two pulses is remarkable. For all frequency ratios $\Omega$ larger values of acceleration are now required to overturn the block (compared with the sinus pulse case). Also, the critical value of the frequency ratio beyond which only overturning without impact can occur has dropped down to about 4. The beneficial effect of the cosine pulse with respect to the sine pulse is attributed merely to the phase shift of $\pi/2$.

Moreover while cycloidal pulses are reasonable idealizations of near-fault ground motions, they cannot fully capture the effect of a slight *asymmetry* inherent to near–fault pulses. The "Ricker wavelet" has a distinct advantage in this respect, and is thus employed here to excite the rectangular block in rocking oscillations (with $r$=0.8). As seen in the overturning spectrum plotted in Fig. 3(c), more failure loops "appear" in this case. Also there is no distinction between overturning with one or no impact as derived from the time-histories of Fig.4. The difference between two "neighbouring" loops is now in the direction of toppling.

### 3.3 Overturning potential of large structures

An important question is whether high-rise buildings or tall bridge piers may safely uplift from their foundation under very strong shaking. Although such tall structures are unlikely to behave as rigid blocks, and their (unavoidable) flexibility is a favourable factor, the rigid block assumption may give a conservative glimpse

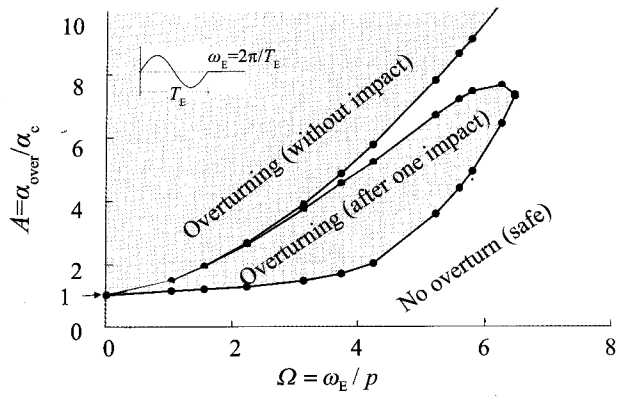


(a) One-cycle sinus pulse

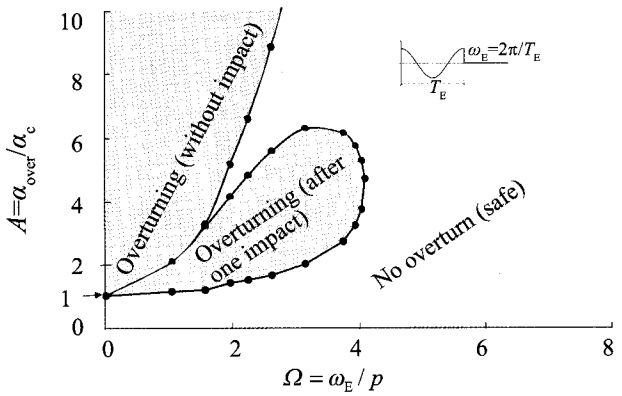


(b) One-cycle cosinus pulse

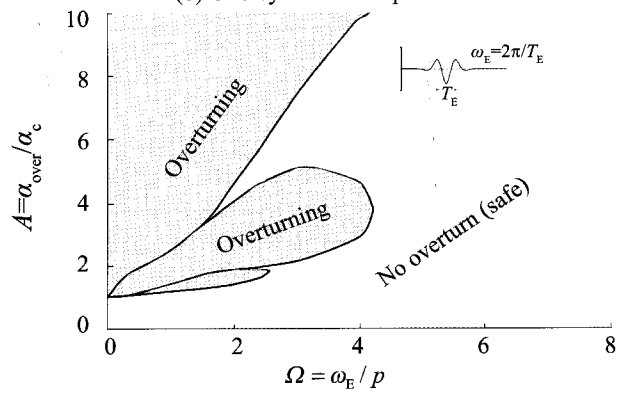


(c) Ricker pulse

**Fig. 3 Overturning amplification ratio (i.e. ratio of dynamic overturning acceleration, $\alpha_{over}$ to the pseudostotic overturning acceleration $\alpha_c$ ) for slender blocks under different pulses compared by : (i) numerical integration of equation of motion (circles) and (ii) the analytical formula derived by Makris and Zhang (solid lines). The coefficient of restitution is 0.8.**

on the threat of overturning. The beneficial effect of increased block size to overturning response is already known. However, with very tall and slender buildings, the slenderness ratio $h/b$ is also large.

The interplay between slenderness and size regarding overturning is clarified with the help of a rectangular block of a constant half-width $b$. In the plots of Fig. 5 the height of the block is gradually increased so that both its slenderness ($h/b$) and its frequency parameter ($p$) keep rising. Initially, a block of $b = 0.5$ m and $h = 1.0$ m is set on rocking under a long-duration one-cycle sinus pulse of $T_E = 0.8$ sec; to topple it, a peak ground acceleration of 0.7 g is needed. By increasing $h$ by a mere 1 m, the overturning acceleration drops to 0.35 g — an example of detrimental influence of slenderness. However, as the height of the structure is further increased, the decrease of the overturning acceleration diminishes and the beneficial effect of the size parameter gradually takes over. Paradoxically, after reaching a minimum about 0.18 g the overturning acceleration tends to increase, not decrease, with increasing height and slenderness! All that happens is that the size effect overshadows the influence of the slenderness and becomes the prevailing parameter on the overturning response. Hence for a sufficiently tall structure of a certain width, the more slender is made the less vulnerable to overturning it will be! Thus, we can explain why large slender structures survive toppling even under severe seismic shaking. In the experimental work of Huckelbridge and Clough (1978) it was made clear that for a practical building, transient uplifting response would in no way imply imminent toppling.

### 3.4 Resemblance of near-fault ground motions with idealized pulses

The resemblance of near-fault ground motion with cycloidal symmetric pulses has been demonstrated by Anooshehpoor *et al.*,(1999), Makris and Roussos (1998; 2000). Asymmetric pulses can be represented with a Ricker or a T-Ricker wavelet. For example the directivity affected Düzce record (in the Kocaeli 1999 earthquake) is compared with a Ricker wavelet ($A_{PG}$=0.28g and $T_E$=1.3s) in Fig. 6. The two time histories excite in rocking a slender block ($\theta_c$=0.2rad) for different values of the period parameter $T_P=2\pi/p$. The resulting spectra of peak rotational angle $\theta_{max}$ and of minimum acceleration level for overturning (derived by scaling up and down each motion). Evidently the simple Ricker pulse can simulate the long-duration pulse inherent in the Düzce record for all values of $T_p$. This almost excellent agreement (with respect to rocking) of the Düzce record with a simply fitted Ricker wavelet indicates that the rocking and overturning is practically unaffected by the high-frequency acceleration peaks that are ever present in every strong accelerogram.

## 4 Elements of neural network analysis

### 4.1 Introduction: the need

As it was demonstrated in the preceding paragraphs, with near–fault type of ground shaking the block uplifting–overturning behavior is sensitive not only to the amplitude and frequency characteristics of the excitation, but moreover to the presence in the excitation of crucial

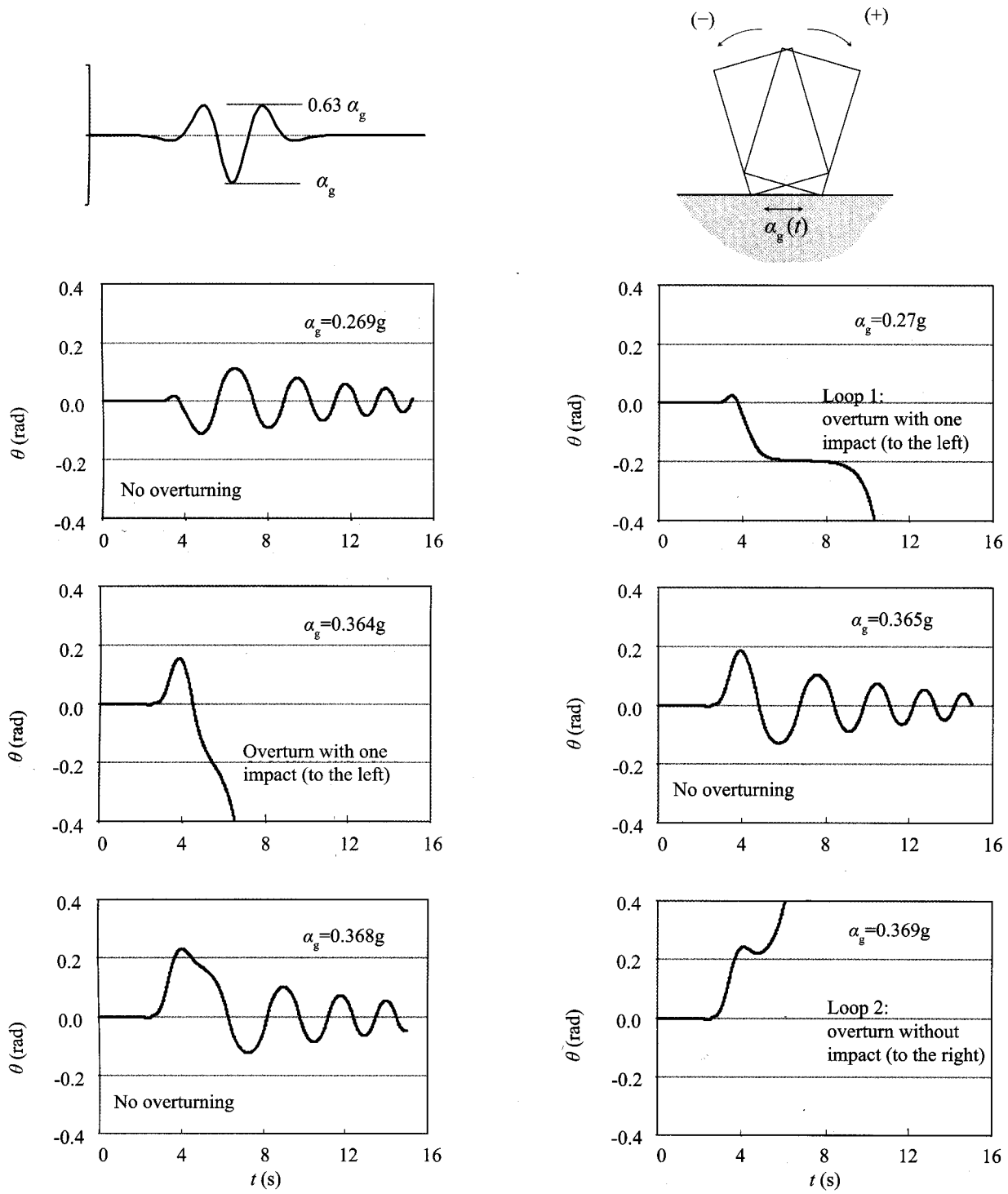


**Fig. 4 Time-histories of the rocking response for a rectangular block with $2b$ = 1 m and $2h$ = 5 m subjected to a Ricker-wavelet excitation of $f_E$ = 0.53 Hz. The coefficient of restitution is 0.89 (elastic impact).**

long–duration pulses. Even the sequence of such pulses is dominant (compare the difference in response to *sinus* and *cosinus* excitation). Predicting such important "details" of a ground motion is clearly an uncertain if not formidable task. In addition, the computational effort of a complete parametric study of this nonlinear vibration problem is not a routine operation. All these make it desirable to explore the feasibility of alternative approaches that allow a quick simplified determination of the ground motion dependent risk of overturning.

The latter task can be formulated as a pattern recognition problem. Of the numerous techniques that are available for such a problem, artificial neural network modeling seems the most prominent. Several studies have been already published utilizing artificial neural networks as an alternative method for such problems

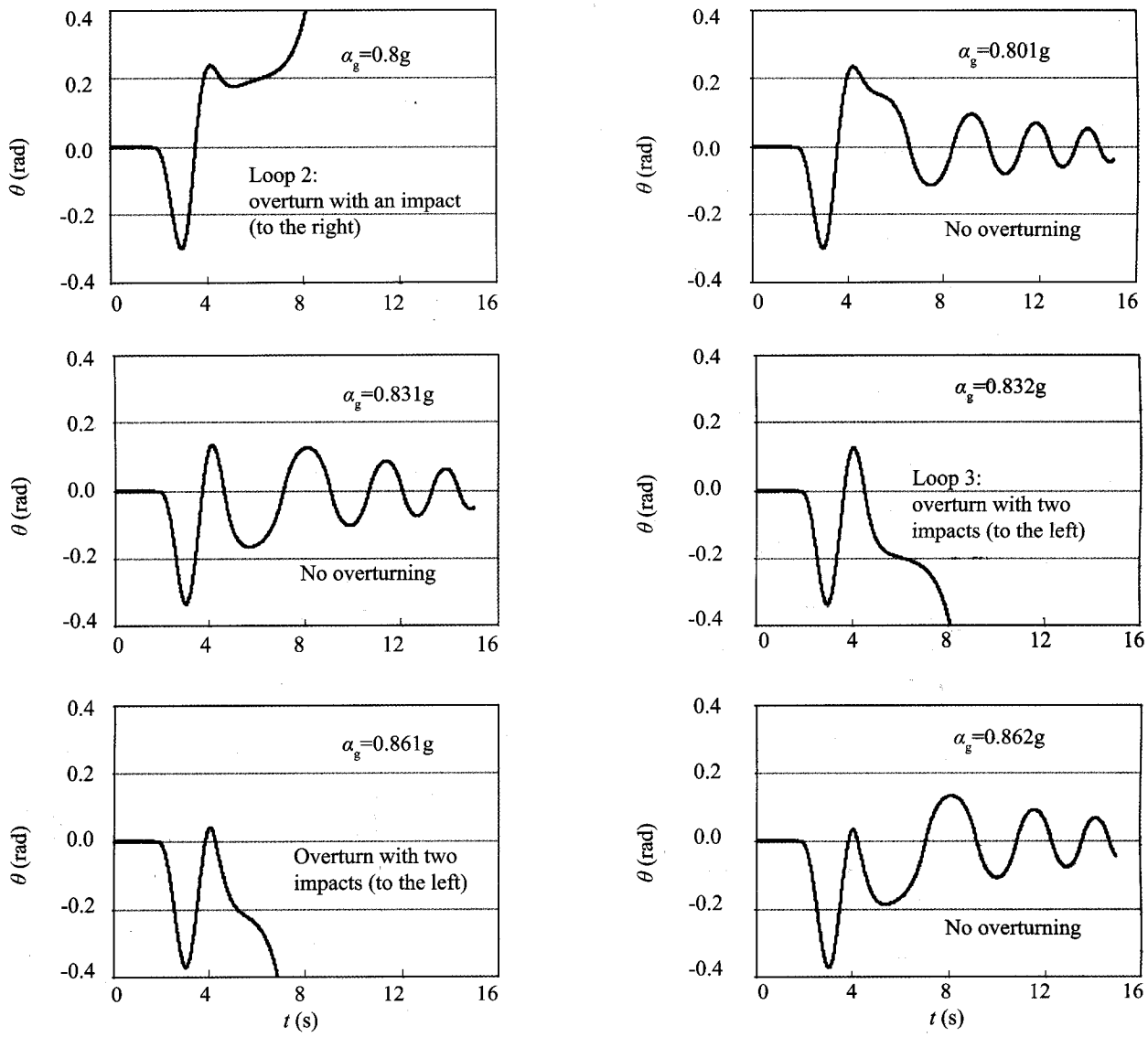


**Fig. 4 (continued)**

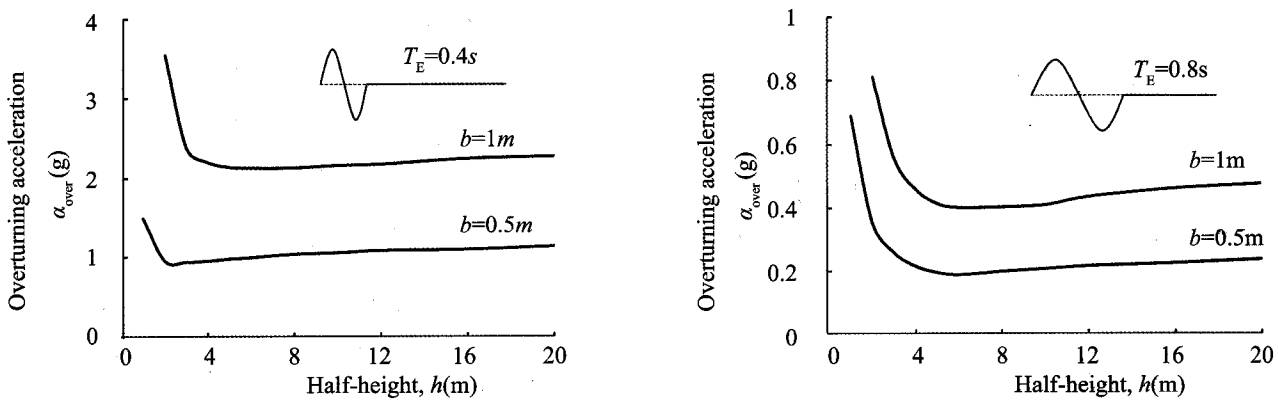


**Fig. 5 Overturning spectra with respect to the half-height *h* for blocks with half-width 0.5 m and 1 m subjected to a one-cycle sinus pulse of period 0.4 sec (left) and 0.8 sec (right).**

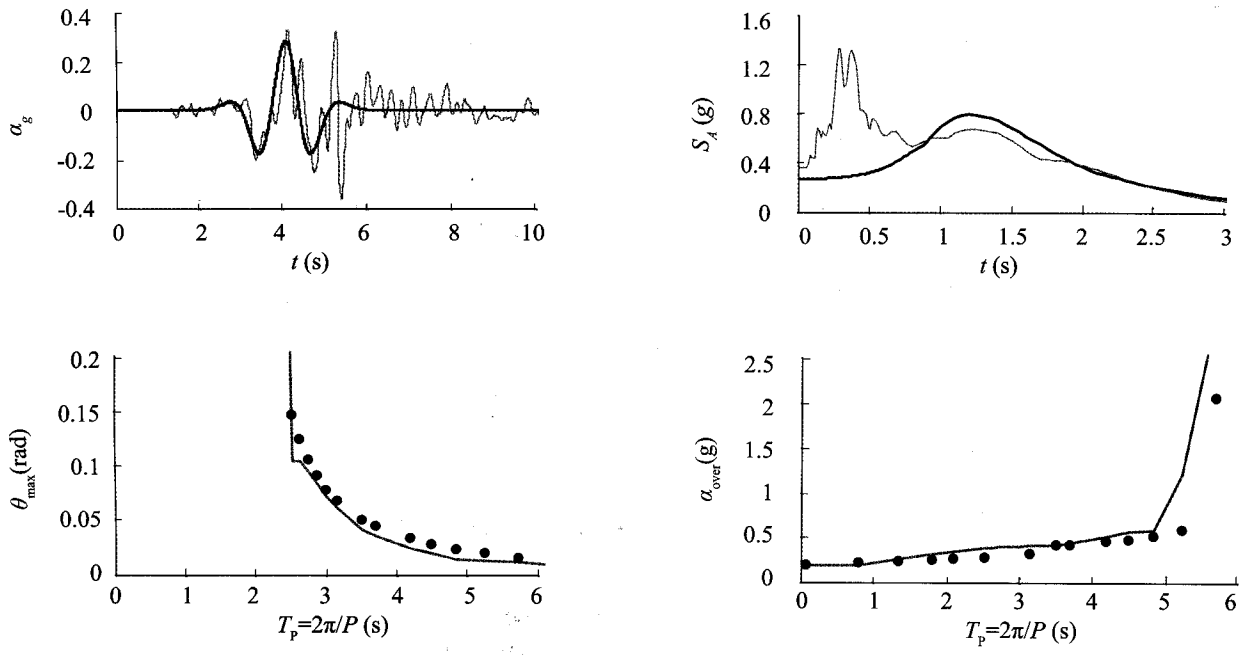


**Fig. 6 Rocking and overturning spectra for blocks with $h/b$ = 5 (critical angle $\theta_c$ = 0.2 rad) subjected to the time-histories of: (a) Düzce, in the Kocaeli Earthquake (plotted with gray solid lines) and (b) a Ricker wavelet (plotted with black solid lines and circular dots).**

as liquefaction (Tung *et al.*, 1993; Goh, 1994; Wang and Rahman, 1999; Baziar and Nilipour, 2003), soil amplification in two dimensions (Faccioli *et al.*, 1998; Hurtado *et al.*, 2001), response of seismic isolation systems (Burton *et al.*, 1996), cyclic material behavior (Ghaboussi *et al.*, 1991) correlation of geotechnical parameters (Akbulut *et al.*, 2004), and earthquake hazard analysis (Habibagahi, 1997; Giacinto *et al.*, 1997).

One of the main advantages of a neural network modeling against other conventional numerical models is that, after the "network training", an approximate analytical solution can be derived even for complicated problems.

An artificial neural network is developed in this study for predicting the overturning response of rigid blocks subjected to near–fault type seismic motions at their base. The neural network analysis leads to a closed–form analytical expression for the overturning acceleration of the rigid block as a function of its geometric properties and the features of the aforementioned idealised pulses. The expression is used to parametrically investigate the problem and is subsequently applied to measure the "destructiveness" of recorded near–fault accelerograms measured in terms of the produced rocking response.

### 4.2 The multi layer perceptron neural network

There are several types of neural network models. A multi layer perceptron (MLP) for pattern recognition is developed in this work for studying the overturning response of rigid blocks to near–fault type seismic motions.

The basic architecture of a multi layer neural network is shown schematically in Fig 7. An MLP network consists of at least three layers: (a) the *input layer* that receives the vector of input, variables of the problem, and passes the information to the network for processing, (b) the *hidden layer* which is a layer of neurons that receives information from the input layer and processes it in a hidden way to the posterior hidden layer or to the output layer, and (c) the *output layer* that receives processed information and produces the response of the system. In a *feed forward* network the units in each layer are not allowed to be inter-connected, whereas each layer can be connected only with the most posterior layer.

Each layer has a weight matrix, $\boldsymbol{w}$, a bias vector, $\boldsymbol{b}$, and an output vector, $\boldsymbol{y}$. Each element of the input vector, $\boldsymbol{x}$, is connected to each neuron input through the weight matrix, $\boldsymbol{w}$. The neuron output, $o$, is a scalar number; it is a nonlinear function (known as the *transfer* or "*activation*" function) of the sum of the outputs of all neurons in the most anterior layer (the neuron input net):

$$o_j\left(net_j\right) = f\left(\sum_i w_{ij}x_i + b_j\right) \tag{8}$$

The neuron outputs of a layer, form the layer output vector, $y$.

The effectiveness of a neural network to simulate highly non–linear problems is partially attributed to the transfer function used for processing the output of a neuron. There are several types of transfer functions, the appropriate choice of which depends strongly on

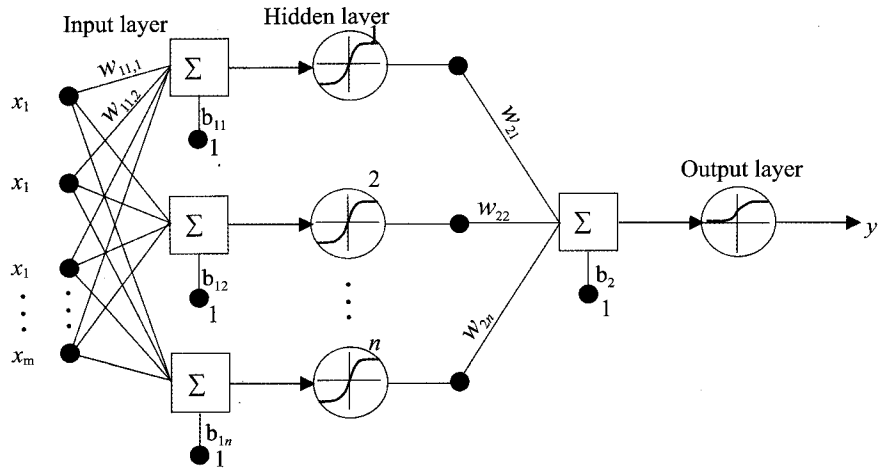


**Fig. 7 Schematic illustration of the architecture of a multi layer perceptron (MLP) feed forward neural network**

the nature of the problem and the type of employed neural network. For function approximation problems a combination of the *symmetric sigmoid* (i.e., the hyperbolic tangent) function

$$f(x) = \tanh(x) \tag{9}$$

for the hidden layer units with the linear function for the output layer units is usually the most promising. However, for pattern classification problems the *logistic sigmoid* (S–Shaped function),

$$f(x) = \frac{1}{1 + \exp(-x)} \tag{10}$$

shall be used as the activation function of the output layer units, instead of the hyperbolic tangent.

The topology of a network (number of the hidden layers and units), affects strongly the result. Theoretical results indicate that a network with two hidden layers and enough hidden units can approximate any nonlinear function to any required degree of accuracy. In other words, any function can be expressed as a linear combination of components containing hyperbolic tangent functions. However, having too large a hidden layer or too many hidden layers can substantially degrade the network's performance.

Several algorithms have been used for determining the optimum topology of a neural network given a specified problem, the most promising of which are the *genetic* and *direct search* algorithms. Nevertheless, network architecture with satisfactory performance can also be developed using trial and error methods (growing and pruning networks). This is the method we adopted in this work

### 4.3 Learning rule

The learning rule is an algorithm that is used to adjust the weight and biases of the network to achieve the desired network behavior. The back–propagation rule is the most popular and has been successfully used to train multi layer networks for function approximation and pattern classification. According to this rule the network weights and biases are adjusted in order to minimize the error (or performance) function of the network. The network weight and biases are continuously being updated until the minimization of the network error function. Derivatives of the error function are, first, calculated for the network's output layer and, then, back–propagated through the network until they reach all units of the hidden layers.

The most important features of the back propagation algorithm are the error and the training function. The selection of an appropriate error function depends on the nature of the problem. The mean–squared error is ideal for a function approximation problem, whereas the "cross–entropy" error, in conjunction with the logistic sigmoid as the activation function of the output layer, is the most suitable combination to use in binomial (two–class) or multinomial classification problems.

Several training functions have been developed to be used in conjunction with the back propagation learning rule, which can be classified into three main categories: (a) the gradient descent, (b) the conjugate gradient, and (c) the quasi–Newton algorithm.The quasi–Newton algorithm has been shown to converge faster than the conjugate gradient one (MATLAB, 2000). It is based on Newton's method, but which does not require calculation of the second derivatives of the Hessian matrix, which is a complex and expensive procedure for feed forward neural networks. The Lavenberg–Marquardt optimization algorithm (MATLAB, 2000) is a quasi–Newton algorithm designed to approach second–order training speed without having to compute the Hessian matrix. The Lavenberg–Marquardt training function is used in this work for network training.

### 4.4 Training

Training is the process that repeatedly applies

input vectors to the network and calculates errors with respect to the difference between the target and the output vectors. The weight and bias of each neuron in the network is then updated with the learning rule after each training cycle / "epoch". This procedure is repeated until the network error falls beneath an error goal, or a maximum number of epochs have occurred.

In pattern recognition problems, the network learns during training phase how to classify the patterns (the input variables of the problem) in several significant cases. This could be based either on "expert" opinion, or on the results of conventional numerical analysis, or on experimental and field data. The more "instructive" the training phase, the more reliable the classification provided by pattern recognition algorithms. In the present case the data set for the training phase comprises results from conventional numerical modeling of the problem by the use of Eqs. (2) and (3).

The goal of a satisfactory training, apart from reaching the error goal, is to make the neural network capable of *generalization*. That means that the network performance does not deteriorate significantly if new input data (different to those we use for training) are presented to the network. The inability of a neural network to generalize after the training is called *overfitting*. One method for improving network generalization is to use a network that is just large enough to provide an adequate fit. The larger a network is, the more complex the functions it can create. A very small enough network will not have enough power to overfit the data. Since it is difficult to know beforehand how large a network should be for a specific application, except from the traditional *early stopping* method, several methods have been developed recently (MATLAB, 2000) to prevent overfitting. The most efficient of which are : (a) the Bayesian regularization, (b) the training with noise, and (c) the hybrid training (based on a combination of batch with incremental training). The reader is referred to the MATLAB user's manual for more detailed documentation.

The efficiency of each of the above methods depends on the nature of the problem. No well defined rule exists for whether or not to a specific overfitting method is more beneficial to the network performance than others.

## 5 Neural network analysis and results

### 5.1 Multilayer perceptron (MLP) neural network utilized in this study

The MLP network used in this study, is schematically illustrated in Fig. 8. It consists of three layers. The input layer comprises four input neurons representing the following parameters (patterns) :

- the peak ground acceleration $A_{PG}$,
- the critical acceleration of the rigid block $\alpha_c$,
- the characteristic cyclic frequency $\omega$ of the ground acceleration time history, and
- the frequency parameter $p$ of the rigid block ( $= \sqrt{3g/4R}$ ).

The hidden layer consists of twenty neurons with the symmetric sigmoid as the "activation" function. Since the problem is a binomial (two–class) pattern classification problem, the output layer has a single neuron and binary target values: 1 for overturning of the rigid block, and 0 for not overturning. The *logistic sigmoid* is used as the "activation" function of the output layer. The calculation of the network weights and biases is based on the minimization of the cross–entropy error function, by setting the error goal to be smaller than 1%. Training of the neural network is achieved with the mathematical computer code MATLAB. The batch training method is applied in conjunction with the Lavenberg–marquardt training function (MATLAB, 2000).

The input data base used for training the neural network consists of results from the exact solution of the problem, Eqs. (2) and (3), by setting the coefficient of restitution, $r$, equal to 0.8 (slightly inelastic impact). Specifically, 15000 data points were used for each one of the five trigonometric pulses. To prevent overfitting the network performance is tested for each of the techniques described in Section 3. The "Early Stopping" method was found to give the best results.

The mathematical formulation of the neural network after the training, is expressed as :

$$y = \frac{1}{1 + \exp\left[ -\sum_{i=1}^{n} w_{2i} \tanh\left( \sum_{j=1}^{m} w_{1i,j} \bar{x}_j + b_{1i} \right) - b_2 \right]} \tag{11}$$

where $m = 4$ and $n = 20$ are the numbers of neurons in the input and the hidden layer, respectively. $w_{1i,j}$ and $b_{1i}$ are the weights and biases of the hidden layer, and

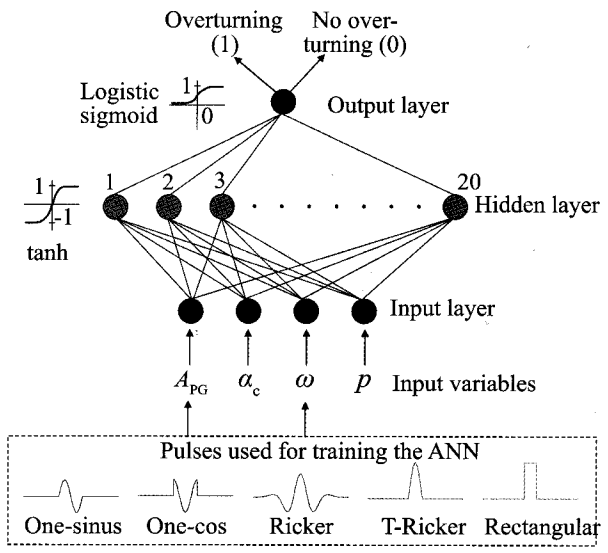


**Fig. 8 Schematic illustration of the neural network used for the overturning response analysis of a rigid block subjected to near–fault type seismic motions**

$w_{2i}$ and $b_2$ the weight and bias of the output layer. The weight and bias values associated with each of the five trigonometric pulses used in our analysis, are presented in Tables 1 through 5. $\bar{x}_j$ is the normalized input vector with respect to the minimum and maximum values of the problem parameters $x_j$ ( $x_1 = A_{PG}$, $x_2 = \dot{\alpha}_c$ , $x_3 = \omega$, and $x_4 = p$), used in the analysis. $\bar{x}_j$ is expressed as a linear function of $x_j$ according to

$$\bar{x}_j = 2 \cdot \frac{x_j - \min x_j}{\max x_j - \min x_j} - 1 \tag{12}$$

The (min, max) values of parameters $x_j$ are ( 0.05g, 4g), (0.05g, 0.30g), (0.628 rad/s, 41.88 rad/s) and (0.5

**Table 1 Weights and biases for the one–cycle sinus pulse**

| Hidden layer | | | | | Output layer | |
|---|---|---|---|---|---|---|
| $w_{1i,j}$ | | | | $b_{1i}$ | $w_{2i}$ | $b_2$ |
| -5.38 | 5.44 | 4.43 | -3.31 | 2.65 | -143.98 | -119.09 |
| -2.51 | -0.78 | 2.88 | -0.28 | -1.99 | 76.68 | |
| -55.52 | 39.22 | 1.34 | -28.01 | 23.26 | -30.71 | |
| 9.66 | -5.15 | 6.76 | -1.63 | 18.30 | -37.11 | |
| -0.56 | 0.46 | -4.04 | -1.69 | -6.07 | 81.67 | |
| -3.35 | 2.79 | 2.43 | 1.77 | 3.05 | -37.89 | |
| 1.88 | -0.02 | -1.80 | 1.21 | 0.67 | 115.75 | |
| -0.69 | 0.41 | 2.76 | -1.32 | 0.65 | -107.28 | |
| 25.67 | -13.56 | -12.76 | 8.02 | 4.98 | -104.92 | |
| -0.07 | 0.07 | 12.45 | -11.31 | -1.00 | -232.08 | |
| -4.38 | 0.03 | -0.12 | 1.18 | -3.55 | -146.00 | |
| -2.11 | 2.26 | 2.74 | -4.54 | -0.87 | -22.00 | |
| 19.78 | -9.85 | -5.46 | 2.43 | 3.86 | 52.41 | |
| -0.74 | -0.37 | -5.37 | 3.67 | -2.07 | 100.30 | |
| 29.20 | -2.41 | -1.21 | -0.05 | 25.58 | 239.48 | |
| -2.59 | 2.91 | -1.67 | 0.68 | 1.11 | -146.01 | |
| 28.26 | -15.02 | -27.18 | 135.56 | 120.80 | 57.43 | |
| 26.87 | -1.80 | 3.44 | -1.99 | 25.55 | -105.58 | |
| 2.66 | 1.76 | 2.16 | -0.45 | 6.40 | 187.92 | |
| -62.86 | 11.02 | 57.01 | -89.68 | -84.24 | 44.97 | |

**Table 2 Weights and biases for the one–cycle cosinus pulse**

| Hidden layer | | | | | Output layer | |
|---|---|---|---|---|---|---|
| $w_{1i,j}$ | | | | $b_{1i}$ | $w_{2i}$ | $b_2$ |
| -2.51 | 0.69 | 25.48 | -5.28 | 18.99 | -78.95 | -109.71 |
| 6.82 | -6.28 | -12.70 | 3.32 | -11.28 | -75.19 | |
| -10.19 | 3.56 | 2.62 | 0.90 | 11.29 | -107.21 | |
| -3.98 | 0.22 | 13.90 | -4.44 | 5.06 | -92.19 | |
| -3.20 | 1.24 | 2.98 | -0.45 | 0.64 | -117.66 | |
| 0.93 | 0.07 | -20.58 | 1.32 | -19.61 | 58.60 | |
| -3.19 | 1.42 | -4.55 | 0.53 | -5.73 | -80.91 | |
| -0.81 | -0.09 | -67.82 | 29.08 | -33.67 | 201.54 | |
| 13.24 | -3.92 | -12.78 | 3.82 | -0.14 | -88.27 | |
| 4.75 | -4.92 | -0.20 | 0.55 | -2.55 | 156.02 | |
| -4.16 | 0.28 | -7.62 | 3.09 | -8.28 | -27.23 | |
| 2.24 | -0.47 | -13.03 | 1.00 | -11.43 | -79.95 | |
| 2.92 | -1.72 | -15.21 | 5.72 | -8.92 | 17.24 | |
| 1.13 | -0.68 | -0.16 | 0.42 | -0.29 | -157.47 | |
| 15.59 | 19.84 | 3.06 | -10.22 | 14.69 | -1.20 | |
| 68.31 | -5.16 | -5.79 | 0.40 | 58.58 | 215.35 | |
| 15.00 | -4.71 | -3.76 | 2.58 | 8.23 | 51.74 | |
| -3.52 | 1.47 | 3.97 | -1.18 | 0.74 | 193.85 | |
| -1.41 | 0.93 | 3.75 | -1.61 | 2.71 | -184.25 | |
| 1.41 | 0.72 | -2.63 | 2.03 | 2.43 | -116.47 | |

rad/s, 5 rad/s), for $A_{PG}$, $a_c$, $\omega$, and $p$, respectively.

### 5.2 Comparison with exact solution

The capability of the neural network model to predict the overturning response of rigid blocks subjected to near–fault type seismic motions is demonstrated by comparison with results from exact numerical solution of the system of the governing Eqs. (2) and (3).

Figure 9(a) plots the overturning acceleration spectrum of a free standing rigid block with a height of 2.58 m and a base width of 0.64 m; these values imply $h / b = 4$, $\alpha_c = 0.25$ g and $p = 2.14$ rad/s. The block is subjected to one–cycle sinus pulse of frequency $f$ (= $\omega$

**Table 3 Weights and biases for the Ricker pulse**

| Hidden layer | | | | | Output layer | |
|---|---|---|---|---|---|---|
| $w_{1i,j}$ | | | | $b_{1i}$ | $w_{2i}$ | $b_2$ |
| -2.46 | 6.97 | 14.69 | -11.34 | -13.97 | 139.07 | -141.25 |
| -2.06 | -0.37 | 6.17 | -1.58 | 3.73 | 53.28 | |
| 1.55 | 0.20 | -4.89 | 1.19 | -2.98 | 95.75 | |
| 0.96 | -0.04 | 5.16 | -3.11 | 1.24 | -138.61 | |
| 0.17 | -1.07 | -49.94 | 38.60 | -4.78 | 209.23 | |
| 42.74 | -24.38 | 4.78 | 22.54 | -13.43 | 7.71 | |
| -5.93 | 4.64 | -7.69 | 4.95 | -0.61 | -110.37 | |
| 1.76 | -0.31 | -8.37 | 0.47 | -7.67 | 109.92 | |
| 13.49 | -23.58 | 37.23 | 31.93 | 19.85 | 1.04 | |
| -9.30 | 0.20 | -1.94 | 0.69 | -11.21 | -259.97 | |
| -1.22 | 0.27 | -13.00 | 9.24 | -2.01 | 167.40 | |
| 81.79 | -39.06 | 41.34 | -6.13 | 49.13 | 1.39 | |
| 6.87 | -4.06 | -7.97 | 2.78 | -0.81 | 6.95 | |
| -12.03 | 2.06 | 1.81 | -0.83 | -9.71 | -37.38 | |
| 7.36 | -4.40 | 13.42 | -6.00 | 8.51 | -15.54 | |
| -184.74 | 57.70 | 17.69 | -7.63 | -99.20 | 31.47 | |
| -24.32 | 4.21 | -23.24 | 6.59 | -37.62 | 14.75 | |
| -2.63 | 1.11 | 3.66 | -1.71 | 2.55 | -89.86 | |
| 87.28 | -6.02 | -32.93 | -37.58 | 59.77 | 2.17 | |
| 4.44 | -2.66 | 0.63 | -0.39 | 0.30 | 180.52 | |

**Table 4 Weights and biases for the T-Ricker pulse**

| Hidden layer | | | | | Output layer | |
|---|---|---|---|---|---|---|
| $w_{1i,j}$ | | | | $b_{1i}$ | $w_{2i}$ | $b_2$ |
| -5.25 | -0.22 | 1.93 | 2.25 | 7.88 | -21.43 | -23.21 |
| -12.80 | 31.92 | 19.25 | 17.92 | -3.75 | 1.41 | |
| -16.04 | 40.28 | 46.34 | -4.70 | -12.12 | -2.49 | |
| -43.11 | 21.36 | 46.52 | 28.29 | 0.53 | -1.00 | |
| -20.81 | 1.70 | -8.48 | -24.31 | -3.17 | -16.54 | |
| 5.45 | -2.71 | 1.09 | -0.03 | 2.38 | 54.10 | |
| 3.47 | -0.71 | -1.82 | 0.82 | 1.86 | 62.68 | |
| 3.83 | 3.08 | 3.03 | -1.07 | 7.15 | -6.27 | |
| -2.37 | 0.22 | -1.79 | 3.53 | 0.93 | 86.55 | |
| -1.33 | 0.72 | -1.84 | -0.22 | -3.46 | 111.36 | |
| -12.03 | 0.52 | -0.49 | 1.33 | -12.13 | -75.82 | |
| -3.02 | 0.40 | 0.36 | -1.33 | -2.51 | -85.94 | |
| -33.19 | -38.28 | 32.12 | 20.55 | 42.02 | -1.97 | |
| 1.61 | -1.31 | -1.63 | 0.32 | 0.63 | 52.90 | |
| 40.44 | 34.26 | -0.09 | -12.24 | 0.33 | -1.82 | |
| 6.50 | 12.62 | 9.21 | 9.03 | 1.97 | 2.85 | |
| -5.11 | 9.37 | 0.80 | 6.09 | -2.51 | 1.72 | |
| -11.58 | 3.46 | 4.96 | 13.40 | -25.10 | -17.07 | |
| 4.97 | -0.04 | 0.58 | -1.37 | 4.57 | 56.65 | |
| -8.91 | -2.11 | 19.95 | -27.04 | 19.37 | -0.89 | |

**Table 5 Weights and biases for the rectangular pulse**

| Hidden layer | | | | | Output layer | |
|---|---|---|---|---|---|---|
| $w_{1i,j}$ | | | | $b_{1i}$ | $w_{2i}$ | $b_2$ |
| -9.21 | 15.30 | -13.56 | 5.86 | 3.27 | -26.07 | -14.09 |
| 2.56 | 8.10 | -4.61 | 1.78 | -9.99 | -19.78 | |
| -9.96 | -1.17 | 9.17 | -7.68 | 5.95 | -34.40 | |
| -13.03 | 6.71 | -6.09 | 1.64 | -6.50 | -25.00 | |
| -10.42 | -2.11 | 4.28 | 0.91 | -9.91 | 37.41 | |
| -5.02 | 1.74 | -0.30 | -1.34 | -4.15 | -81.91 | |
| -1.88 | 1.04 | -7.29 | -0.02 | -6.50 | -25.34 | |
| 11.75 | -2.31 | -4.25 | 3.12 | 8.75 | 65.73 | |
| -0.91 | -0.45 | -4.28 | 7.21 | 3.17 | 136.82 | |
| -8.18 | -18.29 | -0.80 | -23.59 | 1.82 | -2.12 | |
| -5.55 | 5.61 | -7.70 | 3.05 | 3.78 | -24.91 | |
| 15.14 | -5.08 | -1.35 | 1.78 | 9.40 | 57.54 | |
| 7.03 | -0.09 | -16.98 | -0.70 | -11.35 | 75.11 | |
| -9.55 | 0.64 | 7.87 | -2.23 | -3.04 | -86.85 | |
| -9.94 | -3.55 | -0.43 | -1.95 | 4.80 | -16.81 | |
| -25.81 | 1.40 | 3.25 | 0.84 | -20.88 | -72.39 | |
| -12.43 | -0.25 | 3.24 | 1.53 | -7.56 | -35.13 | |
| -54.03 | 3.32 | 3.79 | 0.41 | -47.31 | -98.75 | |
| 41.58 | 1.38 | 4.31 | -2.51 | 45.34 | 94.90 | |
| 11.60 | -1.97 | 4.06 | -1.85 | 10.76 | -23.75 | |

/ 2π). Comparison is given between results from exact solution (crosses) and those computed with the neural network model (solid line). The comparison is generally very good, except to that the neural network modeling can not capture the very narrow safe zone between the two overturning areas, in the frequency range 1–1.7 Hz. This difference is because only a few input data are associated with this narrow zone, which are thus treated as a noise by the neural network during the training process. The effect of this data on the resulting output is ignored by the neural network, in the frame of generalization. Admittedly, however, the practical significance of this small discrepancy is indeed negligible, as engineering design can hardly rely on this zone for a safe design.

The plots in Figs. 9(b)-(e) are as of Fig 9(a), but for the one–cycle cosine, the Ricker, the T–Ricker, and the rectangular pulse, rather than the one–cycle sinus. The comparison is satisfactory and in some cases excellent.

To investigate the destructiveness of the five studied pulses, the overturning acceleration spectra of all of them are compared in Fig 10. The more destructive a pulse, the larger the overturning area (in the frequency domain). The rectangular pulse is obviously the most destructive, followed by the T–Ricker, the one–cycle sinus, the Ricker, and finally the one–cycle cosinus pulse (which is by far the least harmful). This is as anticipated, considering the rather "static" nature of the rectangular and T–Ricker pulses. Note that only the first overturning mode (i.e., after one impact) is possible with T-Ricker and rectangular excitation because of their unidirectional nature.

Having validated the neural network against the exact solution, we utilize it to compute the overturning response of a rigid block for two different sizes (as a combination of parameters $\alpha_c$ and $p$). For a block with $b$ = 0.09 m and $h$ = 0.56 m ($\alpha_c$ = 0.16g , $p$ = 3.38 rad/s), and one with $b$ = 3 m and $h$ = 10 m ($\alpha_c \approx$ 0.30g) , $p \approx$ 0.8 rad/s which are representative values of a cemetery tomb, and a slender 6–story building, respectively. The results associated with each of the five pulses are plotted in Figs. 11(a) to (e), along with the results of the previous case study ($b$ = 0.32 m and $h$ = 1.29 m, i.e. $\alpha_c$ = 0.25 g, $p$ = 2.14 rad/s), for comparison. The latter values are representative of an electrical transformer block (Makris and Roussos, 2000). It is evident from these figures that the larger the block the more difficult is to overturn.

## 6 Application to real records and conclusions

The developed neural network model is further utilized to assess the "destructiveness" of two recorded near–fault accelerograms. To this end, the response of a whole spectrum of rigid blocks (i.e. of combinations of $h$ and $b$) is excited at the base with each of these accelerograms. The combination of slenderness ratios, h/b, and size parameters, $1/p$ ($\sim\sqrt{R}$), that are needed for the block to just fail by overturning are obtained by numerical solution. The results are plotted as $h/b$ versus $1/p$ diagrams, such as those shown in Figs. 11(a) to (e). These diagrams differ from the "Overturning–Accelera tion Amplification" spectra and the "Angle of Rotation" spectra that have been presented so far in this paper, in that the input accelerogram is fixed and no response quantity is plotted – only the "fatal" combination of

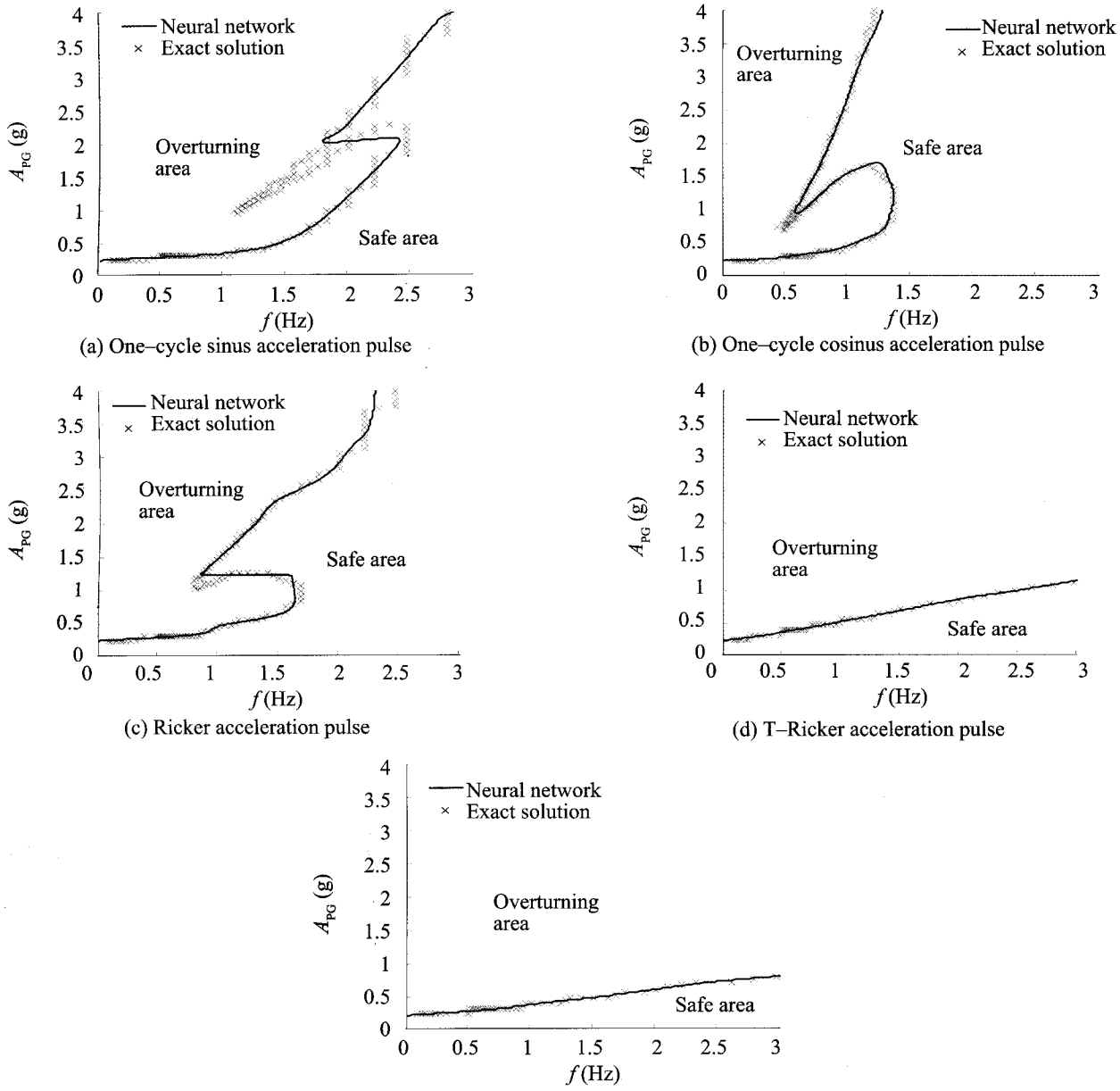


(a) One–cycle sinus acceleration pulse

(b) One–cycle cosinus acceleration pulse

(c) Ricker acceleration pulse

(d) T–Ricker acceleration pulse

(e) Rectangular acceleration pulse

**Fig. 9 Overturning acceleration spectrum of a free standing rigid block with semi–width of $b$ = 0.32 m and semi–height of $h$ = 1.29 m ($a_c$ =0.25 g, $p$ = 2.14 rad/s) and coefficient of restitution $r$ = 0.8 subjected to different acceleration pulses with frequency $f$. Comparison between exact solution and artificial neural network approximation**

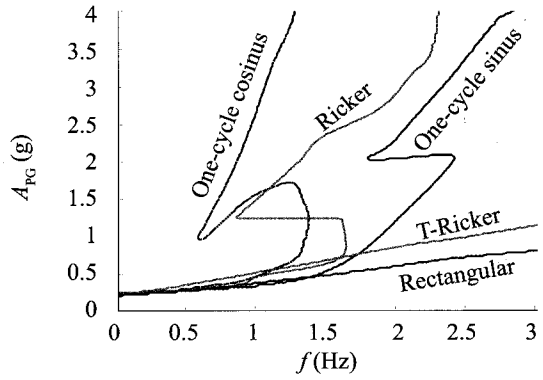


**Fig. 10 Overturning acceleration spectras of a free standing rigid block with semi–width of $b$ = 0.32 m and semi–height of $h$ = 1.29 m ($a_c$ =0.25 g, $p$ = 2.14 rad/s) and coefficient of restitution $r$ = 0.8 subjected to five acceleration pulses with frequency $f$, computed by the artificial neural network**

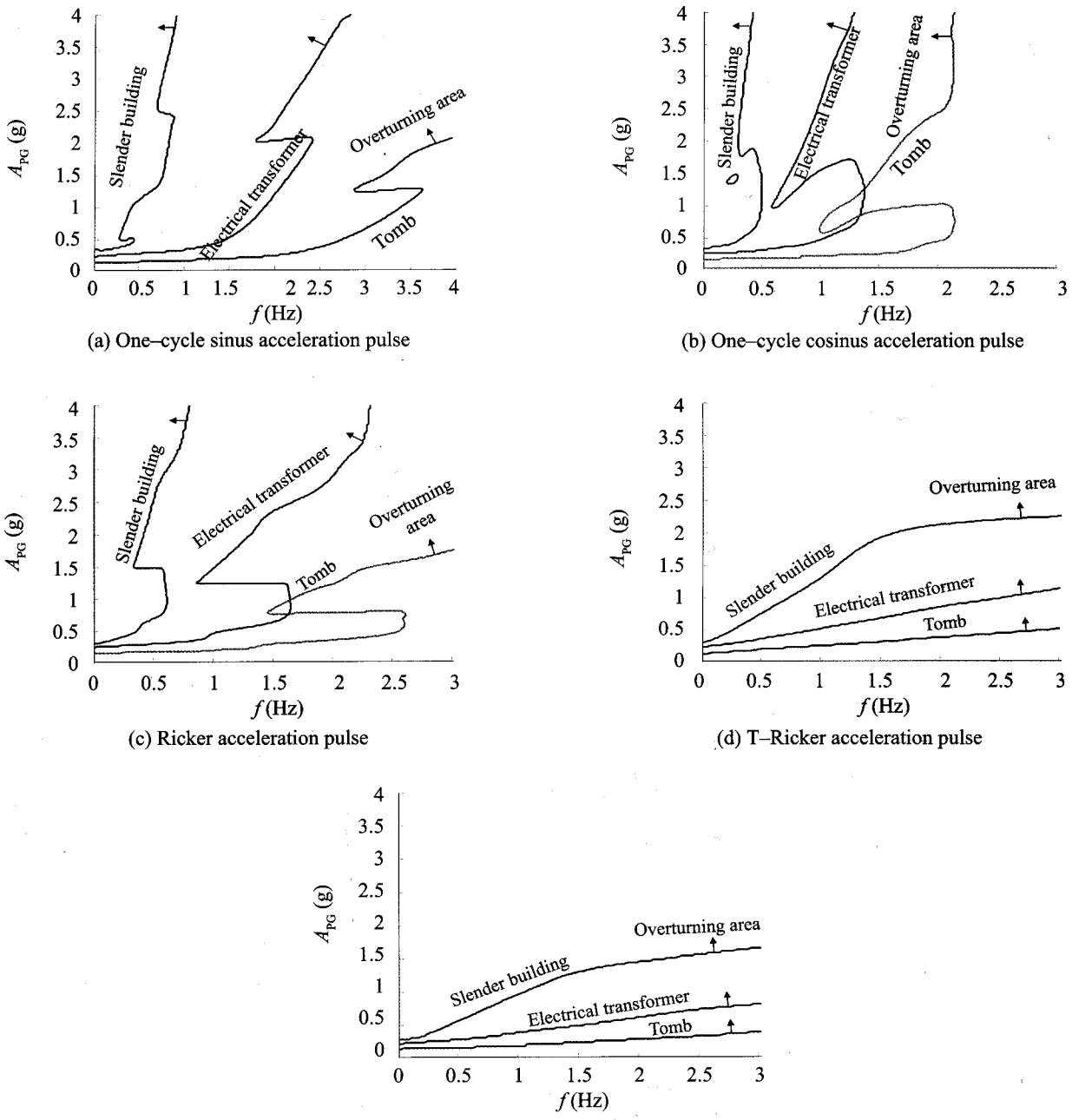


(a) One–cycle sinus acceleration pulse

(b) One–cycle cosinus acceleration pulse

(c) Ricker acceleration pulse

(d) T–Ricker acceleration pulse

(e) Rectangular acceleration pulse

**Fig. 11 Overturning acceleration spectras of a free standing rigid block with three different sizes representative of a (i) cemetery tomb of $b$ = 0.09 m and $h$ = 0.56 m ($\alpha_c$ =0.16 g, $p$ = 3.38 rad/s), (ii) electrical transformer block of $b$ = 0.32 m and $h$ = 1.29 m ($\alpha_c$ =0.25 g, $p$ = 2.14 rad/s) and (iii) slender building of $b$ = 3 m and $h$ = 10 m ($\alpha_c$ =0.3 g, $p$ = 0.76 rad/s), computed with the neural network. The block or the building is subjected to different acceleration pulses at its base**

block geometric parameters $h/b$ and $1/p$.

The two accelerograms investigated are components of: (a) the Düzce record (Kocaeli 1999 earthquake) which is representative of fault–normal ground motions affected by forward–rupture directivity and (b) the Sakarya record (Kocaeli 1999 earthquake) which is representative of fault–parallel motions affected by permanent offset ("fling")

Simple pulses, of the type studied in this paper, are then fitted to these two records. To this end, use Fourier analysis and suitable filtering, along with an optimisation technique. The description of this process lies beyond the scope of this paper. What interest us here is that the following two pulses are obtained :

- a Ricker wavelet with $A_{PG}$ = 0.33 g and $f$ = 0.88 Hz for the Düzce record, as already explained in Fig. 6.
- a T–Ricker wavelet with $A_{PG}$ = 0.33 g and $f$ = 1.27 Hz for the Sakarya record.

The neural network analysis for these two pulses gives the results plotted as a sequence of circular dots

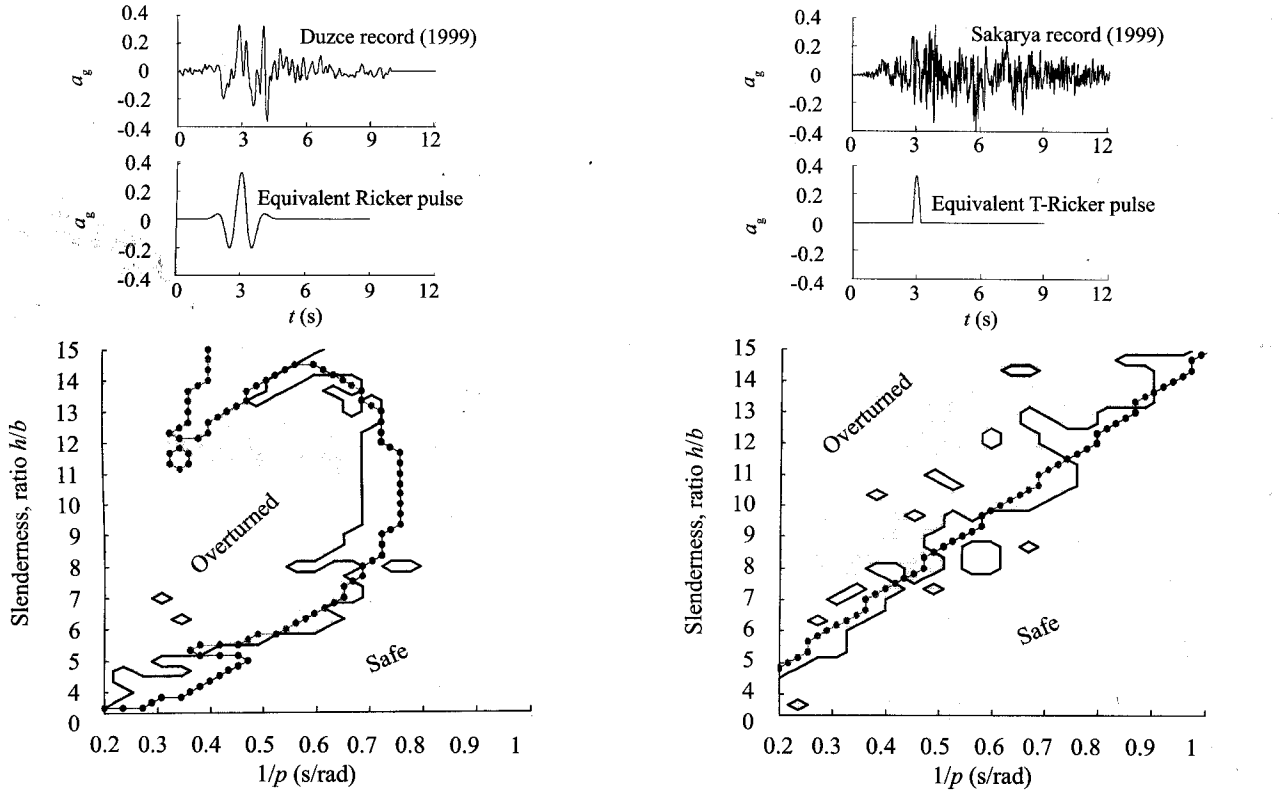


(a) Under two excitations: (i) the Duzce record (Kocaeli 1999 earthquake), and (ii) a suitably fitted ("equivalent") Ricker wavelet

(b) Under two excitations: (i) the Sakarya record (Kocaeli 1999 earthquake), and (ii) a suitably fitted ("equivalent") T–Ricker wavelet

**Fig. 12 Relationship between slenderness ratio and size para-meter (1 / *p*) required for the overturning of a rigid block. Comparison between numerical solution for (i) [plotted with continuous lines] with the neural network results for (ii) [plotted as sequence of circular dots]. The "islands" of the numerical solution represent either unexpected survival of the block when located above the continuous solid line (i.e., within the overturned area), or "premature" overturning when located below the continuous line (i.e., within the safe area)**

in the "fatal combination of *h/b*–versus–1/*p*" diagrams in Figs. 12(a) and (b), respectively; they are compared with the results of the numerical analysis for the two complete records of Düzce and Sakarya (plotted as continuous lines).

The following conclusions can be drawn:

(a) The performance of our neural network modeling (along with the two simple pulses) is quite satisfactory. The results plot as relatively smooth curves, around which the exact numerical results fluctuate. For design purposes, when the details of the ground motion cannot be possibly predicted, use of an appropriate simple pulse with the developed neural network analysis would be the best engineering solution.

(b) The nearly chaotic nature of overturning of a block on rigid foundation subjected to actual ground motions is revealed from the presence of "safe islands" within the Overturned region of the two diagrams, and the rapid fluctuations of the basic curve delineating the "Safe" and "Overturned" regions.

(c) The Düzce record is more destructive than the Sakarya record for blocks with slenderness ratio less than 10, but less destructive for slenderness ratios larger than 10. The undoubtedly richer in high–frequency components Sakarya record increases the risk of overturning of an extremely slender structure.

## References

Abrahamson N (2001), "Incorporating Effects of Near Fault Tectonic Deformation into Design Ground Motions," *A presentation sponsored by the Multidisciplinary Center for Earthquake Engineering Research*, SUNY at Buffalo.

Akbulut S, Hasiloglu AS and Pamukcu S (2004), "Data Generation for Shear Modulus and Damping Ratio in Reinforced Sands Using Adaptive Neuro–fuzzy Inference System," *Soil Dynamics and Earthquake Engineering*, **24**: 805-14.

Anderson C and Bertero V (1986), "Uncertainties in Establishing Design Earthquakes," *Journal of Structural Engineering,* ASCE, **113**: 1709-1724.

Anooshehpoor A, Heaton T, Shi B and Brune J (1999), "Estimates of the Ground Acceleration Point Reyes Station During the 1906 San Francisco Earthquake," *Bulletin of the Seismological Society of America*, **89**(4): 843-853.

Apostolou M, Anastasopoulos J and Gazetas G (2001), "Back-analysis of Sliding and Toppled Structures for the Estimation of Ground Motion During the Athens Earthquake (1999)," *2nd Greek Conference on Earthquake Engineering and Engineering Seismology*, Thessaloniki, Greece.

Apostolou M and Gazetas G (2005), "Seismic Response of Slender Rigid Structures with Foundation Uplift," *Soil Dynamics and Earthquake Engineering* (in press).

Baziar MH and Nilipour N (2003), "Evaluation of Liquefaction Potential Using Neural–networks Land CPT Results," *Soil Dynamics and Earthquake Engineering*, **23**: 631-636.

Burton SA, Makris N, Konstantopoulos IK, and Antsaklis PJ (1996), "Modeling the Response of an Electrorheological Fluid Damper: Constitutive Modelling and Neural Networks," *Intelligent Automation and Soft Computing*, **2**(4): 339-54.

Faccioli E, Paolucci R and Vanini M (1998), "3D Site Effects and Soil Foundation Interaction in Earthquake and Vibration Risk Evaluation," TRISEE.

Ghaboussi J, Garret JH and Wu X (1991), "Knowledge Based Modeling of Material Bbehavior with Neural Networks," *J Engng Mech Div,* ASCE, **117**(2): 132-53.

Giacinto G, Paolucci R and Roli F (1997), "Application of Neural Networks and Statistical Pattern Recognition Algorithms to Earthquake Risk Evaluations," *Pattern Recognition Letters*, **18**: 1353-62.

Goh ATC (1994), "Seismic Liquefaction Potential Assessed by Neural Networks," *J Geotech Engng,* ASCE, **120**(9): 1467-80.

Habibagahi G. (1997), "Reservoir Induced Earthquakes Analyzed via Radial Basis Function Networks," *Soil Dynamics and Earthquake Engineering*, **17**: 53-56.

Hisada Y and Bielak J. (2003), "A Theoretical Method for Computing Near–fault Ground Motions in Layered Half-spaces Considering Static Offset due to Surface Faulting, with a Physical Interpretation of Fling Step and Rupture Directivity," *Bulletin of the Seismological Society of America*, **93**(3): 1154–1168.

Housner G (1963), "The Behavior of Inverted Pendulum Structures During Earthquakes," *Bulletin of the Seismological Society of America*, **53**(2): 404-417.

Huckelbridge AA and Clough RW (1978), "Seismic Response of Uplifting Building Frame," *Journal of Structural Engineering*, ASCE, **104**(8): 1211-1229.

Hurtado JE, Londono JM and Meza MA (2001), "On the Applicability of Neural Networks for Soil Dynamic Amplification Analysis," *Soil Dynamics and Earthquake Engineering*, **21**: 579-91.

Ishiyama Y (1982), "Motions of Rigid Bodies and Criteria for Overturning by Earthquake Excitations," *Earthquake Engineering and Structural Dynamics*; **10**: 635-650.

Kirkpatrick P (1927), "Seismic Measurements by the Overthrow of Columns," *Bulletin of the Seismological Society of America*; **17**(2): 95-109.

Makris N and Roussos YS (1998), "Rocking Response and Overturning of Equipment Under Horizontal Pulse-type Motions," *Technical Report 5*, Pacific Earthquake Engineering Research Center.

Makris N and Roussos YS (2000), "Rocking Response of Rigid Blocks Under Near–source Ground Motions," *Geotechnique,* **50**(3): 243-262.

MATLAB (2000), "The Language of Technical Computing," *Copyright 1984-2000* The MathWorks, Inc.

Milne J. and Omori F. (1893), "On the Overturning and Fracturing of Brick and Other Columns by Horizontally Applied Motion," *The Seismological Journal of Japan*, **1**: 59-86.

Shi B, Anooshehpoor A, Zeng Y and Brune J (1996), "Rocking and Overturning of Precariously Balanced Rocks by Earthquake," *Bulletin of the Seismological Society of America*, **86**(5): 1364-1371.

Somerville P and Graves R (1993), "Conditions that Give Rise to Unusually Large Long Period Ground Motions," *Structural Design of Tall Buildings*; **2**: 211-232.

Somerville P (2003), "Characterization of Near Fault Ground Motions for Design," *American Concrete Institute Conference*, San Diego.

Spanos P and Koh A-S (1984), "Rocking of Rigid Blocks Due to Harmonic Shaking," *Journal of Engineering Mechanics* ASCE; **110**(11): 1627-1642.

Tung ATY, Wang YY and Wong FS (1993), "Assessment of Liquefaction Potential Using Neural Networks," *Soil Dynamics and Earthquake Engineering*, **12**: 325-35.

Wang J and Rahman MS (1999), "A Neural Network Model for Liquefaction–induced Horizontal Ground Displacement," *Soil Dynamics and Earthquake Engineering*, **18**: 555-68.

Wong C M and Tso W K (1989), "Steady-state Rocking Response of Rigid Blocks. Part 2: Experiment," *International Journal of Earthquake Engineering and Structural Dynamics*, **18**: 107-120.

Zhang J and Makris N (1999), "Rocking Response and Overturning of Anchored Equipment Under Seismic Excitations," *Technical Report 6,* Pacific Earthquake Engineering Research Center.